Composite Structures 373 (2025) 119701

Contents lists available at ScienceDirect

Composite Structures

journal homepage: www.elsevier.com/locate/compstruct

Inverse-based multi-step numerical homogenization for mechanical characterization of converted corrugated board☆

Tomasz Garbowski [a,*], Aram Cornaggia [b], Tomasz Gajewski [c], Jakub K. Grabski [d], Damian Mrówczyński [e]

[a] Department of Biosystems Engineering, Poznan University of Life Sciences, Wojska Polskiego 50, 60-627 Poznań, Poland
[b] Department of Engineering and Applied Sciences, Università degli studi di Bergamo, viale G. Marconi 5, 24044 Dalmine, BG, Italy
[c] Institute of Structural Analysis, Poznan University of Technology, Piotrowo 5, 60-965 Poznań, Poland
[d] Institute of Applied Mechanics, Poznan University of Technology, ul. Jana Pawła II 24, 60-965 Poznań, Poland
[e] Doctoral School, Poznan University of Life Sciences, Wojska Polskiego 28, 60-637 Poznań, Poland

ARTICLE INFO

Keywords:
Material identification
Corrugated board
Numerical homogenization
Artificial neural network
Inverse analysis
Finite element method

ABSTRACT

This paper presents a two-step inverse-based numerical homogenization framework for the mechanical characterization of converted corrugated board. The methodology combines high-fidelity 3D simulations with global plate modeling, enabling the extraction of homogenized stiffness parameters that account for imperfections such as fluting flattening and local degradation of paper properties during converting processes. In the first step, a 3D finite element model of a corrugated structure is perturbed to simulate realistic imperfections. The mechanical response is computed for multiple loading conditions. A simplified homogenized plate model is then calibrated using inverse optimization to match the 3D response, resulting in an identified plane stress membrane, bending and shear components known from the standard plate and shell theories of orthotropic materials In the second step, these reference stiffness values are used to inversely identify the geometric and material parameters of the constituent layers. The design variables include fluting geometry and the thickness and orthotropic elastic properties of each paper layer. The optimization reveals which parameters have the strongest influence on global behavior, offering insights into process sensitivity. The proposed method provides a robust and efficient path from microstructural features to global mechanical performance, suitable for design and quality control in industrial packaging applications. The framework may also be extended using neural networks for rapid estimation, enabling integration into broader simulation pipelines.

1. Introduction

Corrugated board is one of the most widely used materials in the packaging industry due to its excellent strength-to-weight ratio, low cost, and recyclability [1–3]. The most common three-layered board is typically composed of a fluted corrugated core sandwiched between two flat linerboards, resulting in a lightweight structure with complex mechanical behavior. The anisotropic nature of the material [4], along with the influence of the geometric configuration and constituent material properties, makes its mechanical characterization a nontrivial task [1,5,6]. Therefore, special numerical techniques must be used, such as numerical homogenization.

From a general viewpoint, in computational mechanics, numerical homogenization is a well-established approach, employed to estimate the effective macroscopic behavior of materials with complex microstructures. In the context of layered or periodic structured natural/artificial materials, such as corrugated board, classic homogenization techniques such as the asymptotic expansion method, first-order and higher-order periodic homogenization, and RVE modeling are commonly employed; some application examples can be found in [7–10], specifically for corrugated board panels and packages. These approaches allow a reduction in computational complexity by substituting the detailed microstructure with a homogeneous equivalent model, while offering and effective, sufficient level of mechanical detailing and structural behavior description. In particular, for computational modeling of shell-like structures, such as those typically employed

☆ This article is part of a special issue entitled: 'Advanced materials models' published in Composite Structures.

* Corresponding author.
E-mail address: tomasz.garbowski@up.poznan.pl (T. Garbowski).

https://doi.org/10.1016/j.compstruct.2025.119701
Received 10 May 2025; Received in revised form 23 September 2025; Accepted 25 September 2025
Available online 28 September 2025

in corrugated board structural components, first-order homogenization methods have been proposed, among others, by Buannic et al. [11], Biancolini and Butti [8], and Talbi et al. [12]. Further developments have been searched, for higher-order homogenization, with effective more refined modeling by Tran et al. [13], Al Jahwari and Naguib [14], and Khakalo and Niiranen [15]. Relevant application examples of such homogenization strategies can be additionally found, with specific focus to the asymptotic expansion method (see, e.g., [16,17]), and to RVE modeling (see, e.g., [18,19]).

For corrugated board materials, various numerical and analytical homogenization approaches have been developed. Early models used beam or shell theories to represent the fluted layer, coupled with equivalent orthotropic plate formulations for the entire structure [8]. More advanced methods incorporated 2D or 3D RVEs that explicitly captured the corrugated geometry to extract stiffness tensors under different boundary conditions [20]. However, such techniques are typically limited to unconverted configurations of cardboards and are not yet suitable to capture and assess imperfections or production process-induced heterogeneities.

In order to delve into difficulties of structural assessment and identification, following another branch of computational mechanics, inverse methods aim at estimating unknown model parameters by minimizing the error between simulated responses and experimental or reference data (see, e.g., [21–23]). These methods have been extensively applied in material modeling, particularly when direct measurement of parameters is impractical (to complex or for innovative materials) or when constitutive models need to account for multi-axial and highly non-linear behaviors, e.g., anisotropy, plasticity, damage, fracture and delamination [24,25].

Within such a framework, optimization-based inverse techniques, including mathematical programming, artificial intelligence and evolutionary algorithms, are often used in combination with finite element (FE) simulations to perform model calibration. In multi-scale problems, inverse methods have been applied to relate experimental data with homogenized models, enabling parameter updates based on macroscopic tests (see, e.g., [9]). This strategy makes them highly suitable for the current context, where mechanical behavior may be altered by conversion processes due to production of the cardboard and is not directly inferable from constituent material data (see, e.g., [26]).

Numerous studies have addressed the mechanical modeling of corrugated board under various loading conditions, such as tensile, bending, shear, and compression, namely referring to tests such as: Edge Crush Test (ECT), four-point Bending Tests (BNT) in both the Machine (MD) and Cross-machine Directions (CD), Shear Stiffness Tests (SST), and Transverse Shear Tests (TST). Cardboard models often highlight the strong anisotropy of the material and the sensitivity of mechanical behavior to the fluting geometry, paper grades, temperature, and relative humidity content [6,27–30]. Analytical and numerical homogenization methods have been used to simulate packaging structures, such as boxes or panels, under realistic conditions (see, e.g., [31–37]).

Nonetheless, modeling converted corrugated board introduces additional challenges, both form mechanical and computational standpoints. Conversion processes such as creasing, die-cutting, and folding introduce local damage, stiffness degradation, and geometric discontinuities [26,38]. Recent efforts have tried to capture these effects using damage mechanics models or empirical degradation factors applied ad hoc [39–43], although, such approaches typically are not generalizable across different geometries or loading cases.

To address these limitations, a research path may integrate multi-scale modeling with inverse parameter identification, allowing models to adapt to changes in structural integrity introduced during conversion. Still, most of these methods are in their early stages and are rarely applied in a systematic, iterative framework like the one proposed in this study. The literature highlights the growing need for homogenization approaches that are both accurate and adaptable to real-world material modifications. While classic homogenization techniques and inverse methods are individually well-established, their combination in a multi-step framework delves toward an innovative approach, particularly for complex layered systems like converted corrugated board. This research addresses this gap by proposing an inverse-based numerical homogenization methodology capable of capturing both material anisotropy and possible conversion-induced alterations, in an effective and robust manner.

The intrinsic complexity of corrugated board is further exacerbated by the converting process, which refers to board materials after they have undergone industrial processing operations such as cutting, folding, gluing, creasing, and printing. These conversion processes introduce localized deformations, residual stresses, and often irreversible damage in critical regions. As a result, the effective mechanical properties of the board, and consistently the homogenized numerical properties, can deviate significantly from those of the original flat panels [39,44–46]. Accurate modeling of such behavior is essential for predicting performance in end-use applications, such as packaging design, structural optimization, and failure analysis.

Traditional modeling approaches include fully resolved finite element models that explicitly simulate the geometry of the corrugation, as well as classic homogenization methods that aim to derive effective material properties for macro-scale simulation. While the former offers high fidelity, it is computationally expensive and impractical for large-scale applications. On the other hand, classic homogenization often fails to capture the influence of conversion-induced features and microstructural heterogeneity [12,39].

In order to bridge this gap, this paper presents a novel inverse-based multi-step numerical homogenization framework aimed at the mechanical characterization of converted corrugated board. The proposed approach combines a two-stage inverse modeling technique with a numerical homogenization scheme. At its core, the method involves identifying effective material parameters by minimizing the discrepancy between experimental observations or detailed simulations and the response of a simplified (homogenized) model. This inverse problem is solved iteratively, either by mathematical programming or artificial intelligence methods, allowing for the progressive refinement of the homogenized material behavior across multiple scales. The multi-step structure of the approach allows for a sequential transition from fine-scale geometric modeling to coarse-scale homogenized representations, each step incorporating corrections informed by inverse analysis. This enables the model to account for both intrinsic material anisotropy and conversion-related modifications. Importantly, this method balances accuracy and efficiency, making it suitable for industrial applications where rapid simulation and prediction are critical.

The proposed framework is validated through a series of numerical experiments and comparison with experimental test data measurements. The gathered results demonstrate the method ability to reproduce key mechanical behaviors observed in converted corrugated structures, including stiffness degradation, and direction-dependent strength, by providing an accurate and computationally efficient tool for mechanical material characterization.

2. Methodology

2.1. Overview of the research workflow

The aim of the methodology presented in the paper is to robustly retrieve the converted properties of the cardboard. The overall methodology consists of three key stages: (i) experimental testing (which, in this paper, in Results Section, is replaced by pseudo-experimental approach), (ii) inverse identification of effective stiffness parameters of converted board (Inverse Problem I), and (iii) iterative parameter adjustment to identify board imperfections (Inverse Problem II). Schematically, the procedure was presented in Fig. 1; specifically, Fig. 1(a) represents Inverse Problem I, while Fig. 1(b) reflects Inverse Problem II. In the paper, for development and validation of the methodology, the

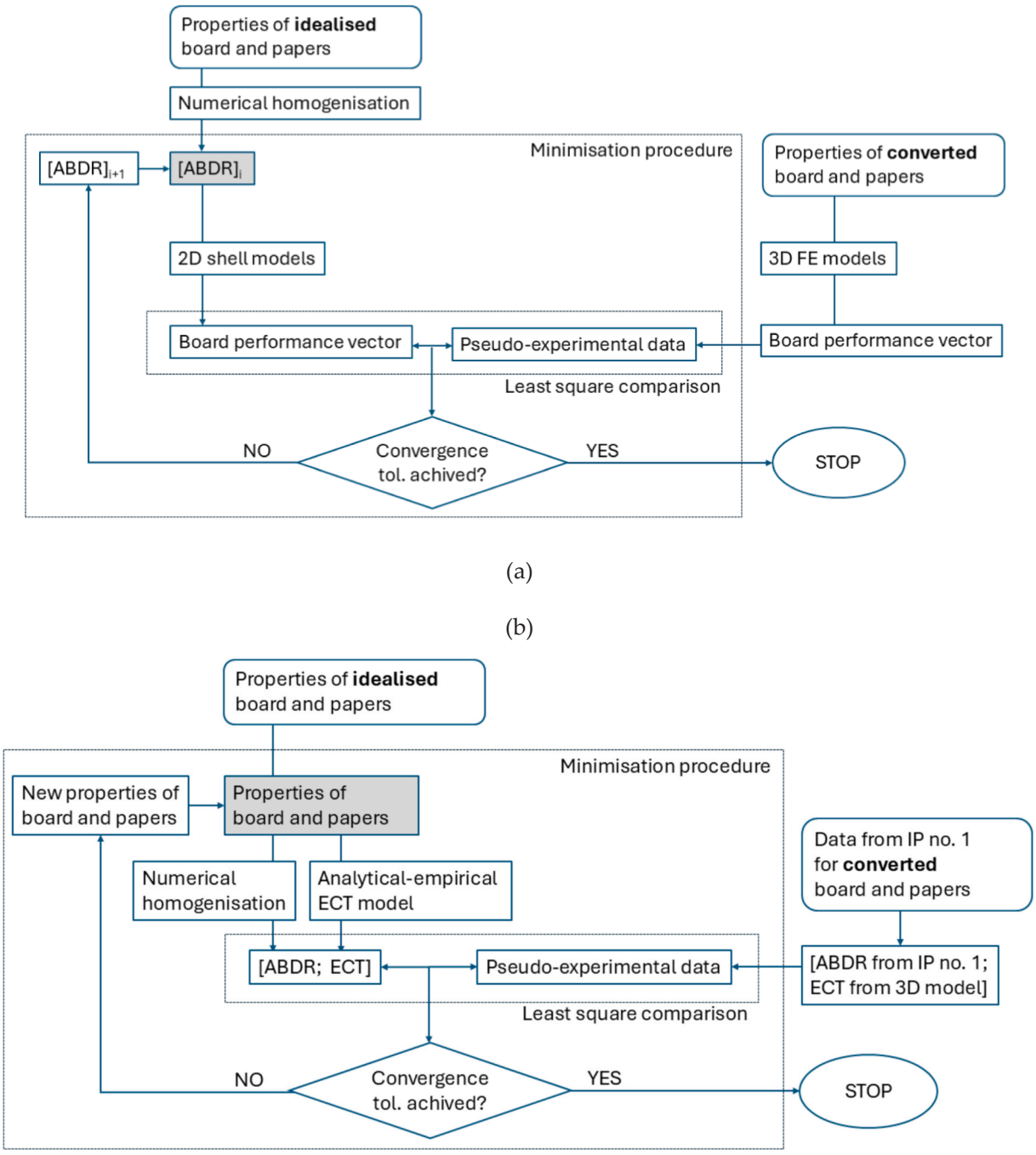

Fig. 1. Graphical representation of inverse-based multi-step mechanical characterization of converted corrugated board: (a) inverse identification of effective stiffness parameters (Inverse Problem I) and (b) iterative parameter adjustment to identify board imperfections (Inverse Problem II).

experimental testing is replaced by a pseudo-experimental approach – see right side of Fig. 1(a) – the experimental data were generated by a numerical method.

In the methodology, the corrugated board samples are tested by six reference mechanical procedures, to determine their effective stiffness behavior under different loading conditions (see Section 2.2). The following tests are used: ECT, which measures the compressive strength of board along the edge, four-point bending stiffness test in machine and cross-machine direction (here abbreviated as BNT-MD and BNT-CD, respectively), which evaluates the flexural rigidity, torsional stiffness test again in machine and cross-machine direction (here abbreviated as TST-MD and TST-CD, respectively), which measures the material resistance to twisting, and SST, which represents the in-plane shear behavior using a square sample. For each test, force–displacement curves were generated by finite element method computations, which served as reference experimental data for numerical calibrations for the left side – Fig. 1(a) and 1(b).

2.1.1. *Pseudo-experimental testing*

Since this study presents the methodology, physical experiments, see Section 2.2, were replaced by high-fidelity 3D FE models of the actual recommended test specimens, which are described in Section 2.3. These models fully replicated the mechanical tests under adequate and realistic boundary conditions.

To simulate real-world production-related defects, the following types of imperfections must be considered:

- paper property modifications;
- fluting geometry deviations;
- paper processing artifacts.

To represent these imperfections, controlled changes were introduced in the FE models, including slight variations in the material parameters—thickness and Young's moduli—of all paper layers, as well as minor deviations in wave geometry, specifically amplitude and wavelength. The magnitude of these variations was set to ± 5 %, resulting in pseudo-experimental force–displacement curves that mimic the variability observed in real tests, while maintaining full control over unknown factors. All types of imperfections were introduced simultaneously in the analysis to increase the difficulty of identifying the true cardboard parameters. A comprehensive discussion of how such imperfections affect the structural response of corrugated board can be found in the study by Mrówczyński et al. [45].

2.1.2. Inverse Problem i – Inverse identification of effective stiffness parameters

A shell-based numerical models of cardboard selected (i.e., without explicit corrugated geometry) was constructed for each test configuration, for more details see Section 2.3. The material input for the models representing the constitutive behavior of the board used was defined through **ABDR** stiffness matrix (plane stress membrane, bending and shear components known from the standard plate and shell theories of orthotropic materials) according to previous works of the group [9,30,33–35,45,46].

The board mechanical response in Inverse Problem I was optimized using a gradient-based inverse procedure (primal–dual interior-point method) combined with least-squares fitting, adjusting the elements of the **ABDR** stiffness matrix. The goal was to iteratively minimize the discrepancy between pseudo-experimental (from 3D FE models, but, in general, from real experimental tests) and numerical (from 2D FE models) curves of test outcomes, allowing for an implicit capture of the imperfection effects. For both models the representative so-called "board performance vector" was defined to be used in least-square fitting (design parameters defined in Section 2.6). The initial design parameters were taken from ideal case of board used, i.e. without production-related imperfections. Finally, in Inverse Problem I, the converged solution represented the board with deteriorated properties due to converting, expressed via **ABDR** stiffness matrix. Since this form is not practically useful, in Inverse Problem II, the numerical homogenization was employed to iteratively retrieve the effective properties of the papers and board geometry.

2.1.3. Inverse Problem II – Numerical homogenization and iterative parameter adjustment

In the Inverse Problem II, a separate RVE model was constructed using initial paper material properties and ideal fluting geometry (with no imperfections), please follow Fig. 1(b). Initial parameters are ideal, i.e., the real-world production effects are excluded. Numerical homogenization was applied to compute the board effective parameters, see Section 2.5, to be used in the Inverse Problem II, for the purpose of accounting for manufacturing-induced deviations of ideal material properties of papers and board geometry.

Also, to include the ECT index in assessing material properties of the board, its influence was incorporated using an analytical-empirical approach, based on findings from a recent study [47]. Its reference value including real world imperfections comes from the ECT full 3D FE model, see Fig. 1(b). Analytical-empirical approach used was briefly described in Section 2.4.

Same as in the previous stage, an iterative inverse procedure was then applied to modify the paper material properties and fluting geometry. The iteration process continued until the homogenized stiffness parameters matched to those from Inverse Problem I and the outcome of the analytical-empirical model of ECT matched to ECT result from 3D FE model. The final, converged parameters are considered to be the effective material properties of paper and fluting geometry, which includes the real-world production-related imperfections through inverse-based multi-step mechanical characterization.

The details of mathematical approach used for minimizations of cost functions, both used in Inverse Problem I and II, were presented in Section 2.6.

2.1.4. Using artificial intelligence to speed up the process

In order to enable fast predictions, which could be used at corrugated board plant, the methodology proposed in this study may also utilize an Artificial Neural Network (ANN) as a surrogate for the computationally expensive finite element analyses, particularly in Inverse Problem I. Using ANN can be especially beneficial in applications such as quality control or box design optimization. Specifically, in Inverse Problem I, the ANN surrogate is used to predict the board performance vector based on the **ABDR** stiffness matrix. Section 2.7 provides details on the implementation and validation of the ANN model used in the study.

2.2. Mechanical testing of corrugated board

In the proposed methodology, the material properties of the boards should be acquired through mechanical tests of the laboratory conditioned samples. However, as a first step of verifying this methodology, the pseudo-experimental approach was used in the study. Despite, this fact the recommended and used in numerical approach mechanical tests were described in this Section to provide the reader with a clear understanding of the tests employed.

Set of corrugated board samples have to be tested in laboratory conditions, i.e., according to TAPPI guidelines (23 °C temperature and 50 % relative humidity) [48,49]. In the methodology, the following experimental procedures for identifying the board properties are used:

- ECT, see Fig. 2(a);
- BNT-MD and BNT-CD, see Fig. 2(b);
- TST-MD and TST-CD, see Fig. 2(c);
- SST, see Fig. 2(d).

Bending stiffness is measured using the four-point bending method. A sample 50x250 mm is loaded in such a way that a constant bending moment and zero shear force occur between the inner supports. However, a shear force remains present between the outer and inner supports, which allows the test to also account for shear stiffness. Bending tests are conducted along both the machine direction and cross-machine direction, at a speed of 37.5 mm/min.

The edge crush test measures the compressive strength of a 25x100 mm sample (typically thicker than 1 mm) when loaded along its edge. For more slender specimens, failure tends to occur due to loss of stability rather than material crushing. ECT is one of the most widely recognized and practically important parameters used in both analytical and numerical evaluations of corrugated packaging load capacity. The test is performed in the cross direction at a speed of 12.5 mm/min.

Shear stiffness is determined using a sample of 85x85 mm, diagonally loaded at opposite corners. Displacements and reaction forces measured at the remaining corners are used to calculate the shear stiffness. Only the linear part of the force–displacement curve is used in identifying the SST parameter. While SST results are sensitive to crushing, they remain reliable even when the samples are significantly damaged.

The torsional stiffness test involves twisting a 30x150 mm sample by a few degrees in both directions. Only the linear segment of the torque–angle curve is considered in evaluating torsional stiffness. Accurate results are ensured by stable sample mounting, a static method for measuring angle and torque, and the relatively large width of the sample, which promotes homogenized material behavior. These tests are conducted in both MD and CD directions.

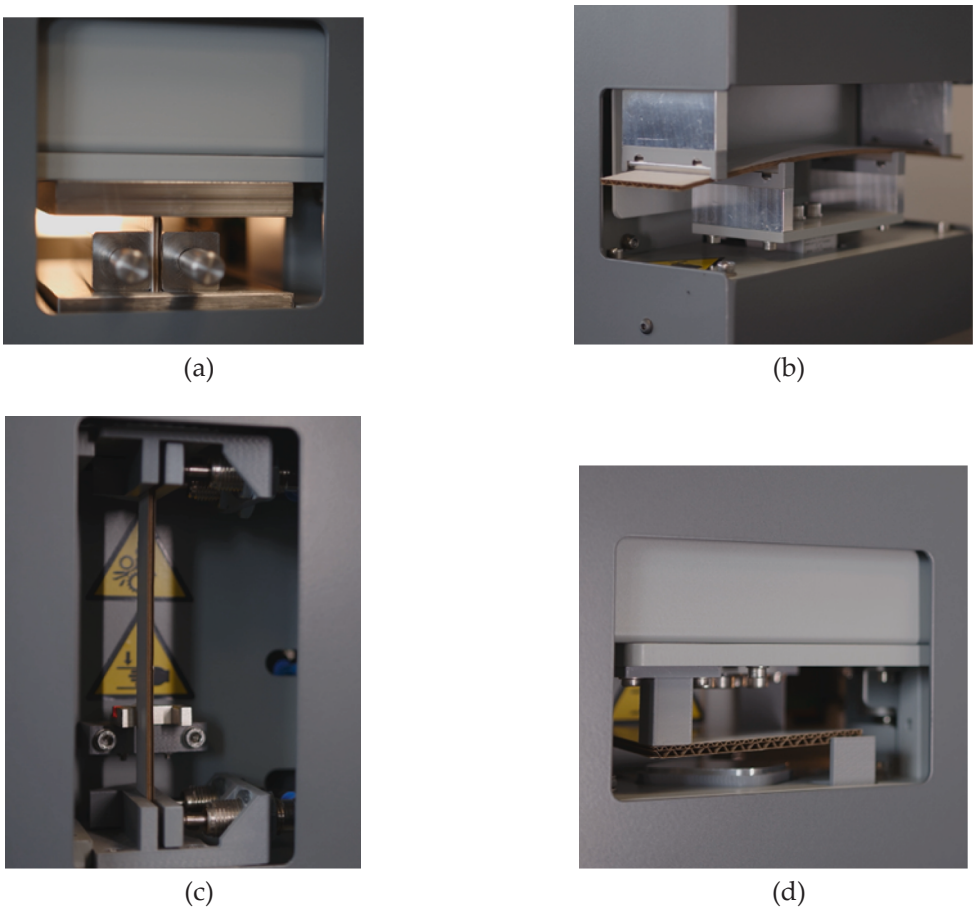

Fig. 2. Test setups used in the experimental study: (a) edge crush test, (b) bending stiffness test, (c) torsion stiffness test and (d) shear stiffness test.

To obtain statistically representative results, five sets of samples should be used for each type of board, assuming a consistent paper sheets (including source supplier) and identical testing conditions. Each sample must be visually inspected to exclude potential damaged or distorted sample.

Only bending and torsion tests are conducted both in the machine direction (along the board flutes) and in the cross-machine direction (perpendicular to the flutes). The testing speed for ECT is set to 12.5 mm/min, in accordance with FEFCO Testing Method No. 8 [50]. For TST, the applied angular velocity is 0.03 rad/s, while for BNT and SST, the testing speed is 37.5 mm/min, therefore all tests may be considered as quasi-static. In Fig. 3, the boundary conditions and loading of cardboard samples in laboratory tests are shown.

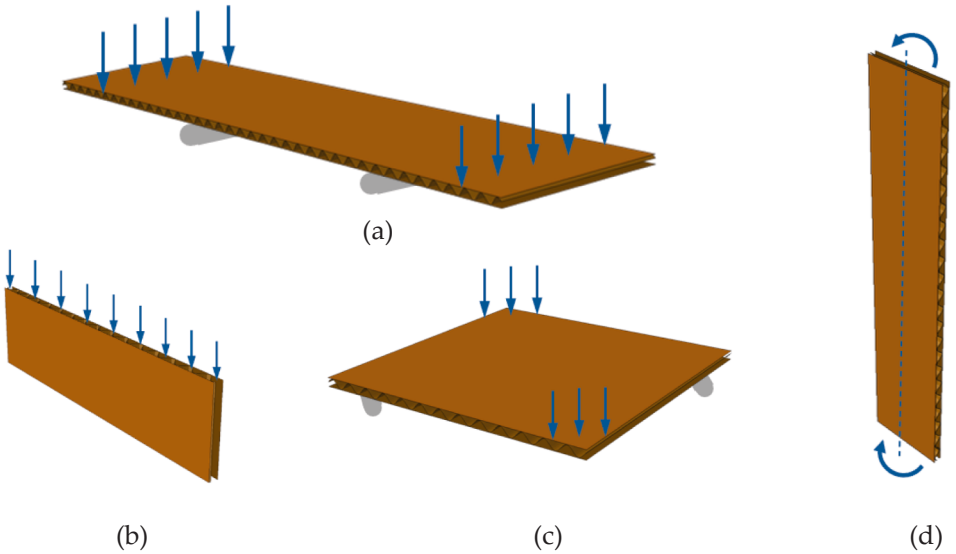

Fig. 3. Sample loading schemes for: (a) bending test, (b) edge crush test, (c) shear stiffness test, and (d) torsional stiffness test.

2.3. Finite element modeling of mechanical tests

Numerical models of the cardboard samples were created using commercial FE software (Abaqus Unified FEA software [51]). In Fig. 3, the load schemes applied in all laboratory tests are presented. The dimensions of the samples were: 50x250 mm in the 4-point bending test, 25x100 mm for the ECT, 85x85 mm in the SST, and 30x150 mm for the torsional stiffness test. Both the 4-point bending and torsional tests were conducted in the machine and cross directions of the cardboard.

The study used B-flute corrugated cardboard with a flute height of 2.46 mm and a period length of 6.5 mm. The 3D model of the cardboard consisted of three paper layers, each assigned material properties listed in Table 1, where t is the thickness, E_1 and E_2 are the Young's moduli in machine and cross directions, ν_{12} is the Poisson's ratio, G_{12} is the in-plane shear modulus, G_{13} and G_{23} are the transversal shear moduli, and σ_0 is the yield strength. These material parameters were also used in the homogenization process to determine the effective stiffness values. The obtained stiffnesses were then applied as material data in the simplified 2D models of the corrugated board.

In all numerical analyses, the four-node quadrilaterals shell elements with full integration (S4 elements, from Abaqus element library) were assumed. In 3D cardboard models, the FE mesh size was equal to 0.5 mm, 3 mm in simplified 2D shells, and 0.2 mm for the RVE models in the homogenization procedure. The results of the numerical analyses in BNT-MD, BNT-CD, ECT and SST were the reaction forces at the supports, and the torque in the TST-ND and TST-CD.

2.4. Analytical-empirical ECT model

The analytical-empirical determination of the ECT value combines precise theoretical modeling with corrections based on real-world observations of corrugated board behavior. In practice, cardboard samples rarely exhibit ideal structural properties – material and structural imperfections often occur, significantly influencing compressive strength. Therefore, a purely analytical approach may overestimate the actual mechanical performance. To address this, an analytical-empirical model is used [47], incorporating both local strength parameters and the effects of buckling in the paper layers. Therefore, the ECT value was calculated from the following formula:

$$ECT = \sum_{i=1}^{n} SCT_i \cdot \alpha_i \cdot \gamma_i \,, \tag{1}$$

where SCT_i is the short-span compression test value of the i-th paper, α_i is the take-up factor of each layer and γ_i is the parameter reducing the static load capacity on compression of each paper layer. This reduction factor is crucial as it includes the buckling behavior of the individual layers, which significantly limits their load-bearing capacity in real conditions. It can be determined from:

$$\gamma_i = SCT_i^{-0.5} \left(\frac{H}{a} \frac{g_i}{b_i} \right)^{0.5} \leq 1 \,, \tag{2}$$

where H is the height of the cross-section, a is the empirical parameter, g_i is the grammage of the individual paper, and b_i is the buckling length of i-th layer. The parameter a was assumed in accordance with the work of Garbowski et al. [47], which value for three-layer cardboards is equal to 52. In Fig. 4, the buckling lengths of the paper layers and the height for three-layer corrugated board are presented. In Table 2, the material parameters used for the analytical-empirical determination of the ECT value of the cardboard are listed.

2.5. Numerical homogenization of corrugated board

In the study, the numerical homogenization was used in order to model the mechanical behavior of corrugated paperboard. The method used here was proposed by Biancolini [8] and later extended by Garbowski and Gajewski [9]. In the method, the equivalence of strain energy between the full (3D) structure, i.e. representative volume element of corrugated paperboard and the simplified shell (2D) model is utilized. Periodically repeating segment of the full structure is used as RVE. The purpose is to simplify RVE to a single shell element with one layer in such a way that the overall behavior of the models, RVE and 2D, are the same. The key assumptions of the described method are presented below; more details may be found in [9].

Displacements at the nodes of the computational mesh can be determined using the Finite Element Method (FEM). The typical equation for FEM analysis takes the following form for external nodes of RVE:

$$\mathbf{K}_e \mathbf{u}_e = \mathbf{F}_e \tag{3}$$

in which, $\mathbf{K}_e$ is the global stiffness matrix with application of static condensation for the external RVE nodes; $\mathbf{u}_e$ is the displacement vector at the external nodes; $\mathbf{F}_e$ is the nodal force vector applied to the external nodes.

In order to neglect, the internal nodes of the RVE model, the static condensation is used for deriving the global stiffness matrix. The unknowns of the FEM system of equation are reduced to selected degrees of freedom, what greatly limits the computational cost. During homogenization process the stiffness matrix is computed only for external nodes by eliminating internal nodes:

$$\mathbf{K}_e = \mathbf{K}_{ee} - \mathbf{K}_{ei} \mathbf{K}_{ii}^{-1} \mathbf{K}_{ie} \tag{4}$$

Subscript e states for external nodes, while subscript i states for internal nodes.

In the method, the strain energy function takes the following form:

$$E = \frac{1}{2} \mathbf{u}_e^T \boldsymbol{F}_e = \frac{1}{2} \mathbf{u}_e^T \mathbf{K} \boldsymbol{u}_e \tag{5}$$

The relations between nodal forces and nodal displacements reads:

$$\begin{bmatrix} \mathbf{K}_{ee} & \mathbf{K}_{ei} \\ \mathbf{K}_{ie} & \mathbf{K}_{ii} \end{bmatrix} \begin{bmatrix} \mathbf{u}_e \\ \mathbf{u}_i \end{bmatrix} = \begin{bmatrix} \mathbf{F}_e \\ 0 \end{bmatrix} \tag{6}$$

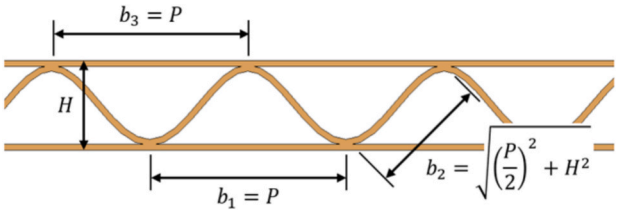

Fig. 4. Cross-section of three-layer cardboard.

Table 1
Mechanical and physical parameters of papers.

No.	t (mm)	E_1 (MPa)	E_2 (MPa)	ν_{12} (–)	G_{12} (MPa)	G_{13} (MPa)	G_{23} (MPa)	σ_0 (MPa)
1	0.16	5600	2800	0.41	1550	100	80	13.8
2	0.13	5400	2600	0.42	1450	90	70	11.4
3	0.16	5600	2800	0.41	1550	100	80	13.8

Table 2
Material parameters for analytical-empirical calculation of the ECT.

No.	*SCT* (N/mm)	*α* (–)	*g* (g/m^2)	*b* (mm)
1	2.2	1.00	120	6.5
2	1.5	1.32	120	4.1
3	2.2	1.00	120	6.5

To achieve the equilibrium between 3D model and 2D model proper nodal displacements are required by taking into consideration the bending and membrane behavior through homogenization. It is essential to relate the displacements and strains in the following way:

$$\mathbf{u} = \mathbf{H}_n \varepsilon \tag{7}$$

in which, $\mathbf{H}_n$ is computed for each node, namely:

$$\begin{bmatrix} u_x \\ u_y \\ u_z \\ \theta_x \\ \theta_y \end{bmatrix}_n = \begin{bmatrix} x & o & y/2 & xz & 0 & yz/2 & z/2 & 0 \\ 0 & y & x/2 & 0 & yz & xz/2 & 0 & z/2 \\ 0 & 0 & 0 & -x^2/2 & -y^2/2 & -xy/2 & x/2 & y/2 \\ 0 & 0 & 0 & 0 & -y & -x/2 & 0 & 0 \\ 0 & 0 & 0 & x & 0 & y/2 & 0 & 0 \end{bmatrix}_n \begin{bmatrix} \varepsilon_x \\ \varepsilon_y \\ \gamma_{xy} \\ \kappa_x \\ \kappa_y \\ \kappa_{xy} \\ \gamma_{xz} \\ \gamma_{yz} \end{bmatrix}_n \tag{8}$$

Now, after [8,9], if we get back to the strain energy, we obtain the following:

$$E = \frac{1}{2} \varepsilon_e^T \mathbf{H}_e^T \mathbf{K} \mathbf{H}_e \varepsilon_e \tag{9}$$

what may be simplified to the form:

$$E = \frac{1}{2} \varepsilon_e^T \mathbf{H}_k \varepsilon_e \{area\} \tag{10}$$

in which:

$$\mathbf{H}_k = \frac{\mathbf{H}_e^T \mathbf{K} \mathbf{H}_e}{area} \tag{11}$$

The matrix obtained, $\mathbf{H}_k$ represents the stiffness matrices corresponding to compression/tension, bending, coupling, and transverse shear stiffnesses, denoted as $\mathbf{A}_{3\times3}, \mathbf{B}_{3\times3}, \mathbf{D}_{3\times3}$ and $\mathbf{R}_{2\times2}$, respectively:

$$H_k = \begin{bmatrix} \mathbf{A}_{3\times3} & \mathbf{B}_{3\times3} & 0 \\ \mathbf{B}_{3\times3} & \mathbf{D}_{3\times3} & 0 \\ 0 & 0 & \mathbf{R}_{2\times2} \end{bmatrix} \tag{12}$$

2.6. Inverse problem formulation and optimization strategy

The mechanical characterization and microstructural identification of corrugated cardboard structures were approached through a two-stage inverse problem, each formulated as a nonlinear constrained optimization task.

2.6.1. Calibration of simplified plate model (ABDR stiffness identification)

In the first stage (Inverse Problem I), a simplified homogenized model of the corrugated cardboard plate was calibrated to reproduce the mechanical behavior observed in detailed three-dimensional (3D) FE simulations. These 3D simulations accounted for structural imperfections such as local buckling of the fluting, small variations in material stiffness, and geometric irregularities, aiming to mimic realistic manufacturing conditions.

The goal of this stage was to identify the effective components of the **ABDR** stiffness matrix (plane stress membrane, bending and shear components known from the standard plate and shell theories of orthotropic materials):

$$\{A_{11}, A_{22}, A_{12}, A_{33}, D_{11}, D_{22}, D_{12}, D_{33}, R_4, R_5\} \tag{13}$$

by minimizing the discrepancy between theoretical predictions of simplified plate tests and the results obtained from full 3D FE analyses. The mechanical tests considered were described in Chapter 2.2:

The optimization problem was formulated as

$$\min_{\mathbf{x}} f(\mathbf{x}) \tag{14}$$

where $\mathbf{x}$ is the vector of **ABDR** stiffness parameters and $f(\mathbf{x})$ is the objective function defined as:

$$f(\mathbf{x}) = \sum_{i=1}^{5} w_i \left(\sigma_i^{2D}(\mathbf{x}) - \sigma_i^{3D} \right)^2 \tag{15}$$

where:

- w_i are the weighting factors assigned to each test,
- $\sigma_i^{2D}(\mathbf{x})$ denotes the theoretical response predicted by the simplified plate model,
- σ_i^{3D} denotes the corresponding response obtained from the 3D FE simulations.

The optimization was constrained by physically meaningful bounds on the stiffness parameters:

$$\mathbf{l}_x \le \mathbf{x} \le \mathbf{u}_x \tag{16}$$

and was solved using a primal–dual interior-point method with Conjugate Gradient (CG) subproblem solver, finite-difference gradient approximations, and multiple initial guesses (multi-start strategy) to mitigate the influence of local minima.

The calibration yielded a set of reference **ABDR** stiffness values $\mathbf{S}^{ref}$, which were then used in the second inverse problem.

2.6.2. Identification of corrugated layer geometry and material properties

In the second stage (Inverse Problem II), the geometrical parameters of the corrugated layer and the material properties of the constituent paper layers (top liner, bottom liner, and fluting) were identified. The aim was to reconstruct the microstructural features that would generate the previously identified reference stiffness values $\mathbf{S}^{ref}$.

The design variables in this stage included:

- fluting geometry:
  wave period P,
  wave height H;
- material properties for each layer:
  – thickness TH,
  – Young's modulus in MD (E_{MD}),
  – Young's modulus in CD (E_{CD}).

The optimization problem was formulated as:

$$\min_{\mathbf{y}} g(\mathbf{y}) \tag{17}$$

where $\mathbf{y}$ is the vector of geometrical and material parameters, and $g(\mathbf{y})$ is the objective function defined as:

$$g(\mathbf{y}) = \sum_{j=1}^{11} \gamma_j \left(S_j^{model}(\mathbf{y}) - S_j^{ref} \right)^2 \tag{18}$$

where:

- $S_j^{model}(\mathbf{y})$ represents the **ABDR** stiffness components predicted by the analytical or semi-analytical model,
- S_j^{ref} are the reference values identified in previous stage,
- γ_j are weighting coefficients associated with each stiffness parameter.

As in the first stage, box constraints ensured realistic values of the physical parameters:

$$\mathbf{l}_y \le \mathbf{y} \le \mathbf{u}_y \tag{19}$$

2.6.3. Solution strategy

A primal–dual interior-point method was employed to solve both optimization problems. This approach, originally introduced by Fiacco and McCormick [52] and further developed by Byrd, Hribar, and Nocedal [53,54] and relies on minimizing a barrier-augmented Lagrangian function:

$$\mathscr{L}(\mathbf{x},\lambda,\boldsymbol{\mu}) = f(\mathbf{x}) + \sum\nolimits_j \lambda_j c_j(\mathbf{x}) + \sum\nolimits_k \mu_k ceq_k(\mathbf{x}) \tag{20}$$

where λ and μ are the Lagrange multipliers for inequality and equality constraints, respectively.

Inequality constraints were enforced through the addition of logarithmic barrier functions:

$$f_{barrier}(\mathbf{x}) = f(\mathbf{x}) - \bar{\mu}\sum\nolimits_j ln(x_j - l_j) - \mu\sum\nolimits_j ln(u_j - x_j) \tag{21}$$

where $\bar{\mu}$ is a positive barrier parameter gradually reduced during the optimization process.

The optimization algorithm used the CG) method to solve the subproblems arising at each iteration, facilitating efficient computation even for larger-scale parameter spaces. Finite differences with a fixed step size were used for numerical gradient approximations, ensuring stable derivative estimates.

The optimization procedure was guided by the following convergence criteria:

- an optimality tolerance on the first-order optimality conditions (10^{-6});
- a step tolerance on the design variables (10^{-4});
- a finite difference step size for gradient approximations (10^{-3});
- a constraint violation tolerance (10^{-6}).

The solution process was initialized from multiple starting points, following a multi-start strategy, to reduce the risk of convergence to local, suboptimal minima. The final identified parameters were those associated with the global minimum of the objective function among all optimization runs.

2.7. Ann-based prediction of effective material properties

A part of the calculation procedure related to prediction of the effective material properties can be replaced by the ANN-based model as presented in Fig. 5. In such the ANN-based model, the input data are elements of the **ABDR** stiffness matrix (10 inputs), and the output vector consists of the effective material properties from mechanical tests described in Chapter 2.2, i.e. BNT in MD, BNT in CD, TST in MD, TST in CD and SST.

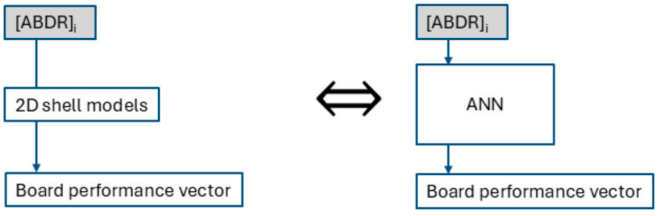

Fig. 5. Replacement of the board performance calculations by ANN model.

The optimization procedures are very time-consuming due to multiple runs of the cost function, which can require performing FE computations, as we propose in this study. However, the numerical simulations can be replaced by the ANN-model trained using the data from these simulations. In the literature, one can find some examples for predicting the strength of specific structures and materials, e.g., the ultimate axial strengths of concentrically loaded concrete-filled steel tubular columns strengthened with carbon fiber-reinforced polymer [55], the bond strength between steel reinforcement and concrete [56], the shear strength of fiber reinforcement bars concrete beams [57], the compressive strength of masonry [58], the tensile strength of fiberglass polymer composites [59]. In this paper, the ANN-based model is employed to predict the performance parameters of converted board. The model was trained using the data from 2D shell model calculations (described in Section 2.3). In this way, the optimization process can be much faster.

In this study, a feedforward multilayered ANN with 2 hidden layers was employed, see Fig. 6. The model has 10 inputs and 5 outputs. Each hidden layer consists of 10 neurons with tangent sigmoid transfer function. The output layer consists of 5 neurons with linear transfer function as 5 outputs of the ANN-model are calculated (effective material parameters). The data used for training was divided into training, validation, and tests sets. In general, the training and validation sets are used during the training process. The training set is used directly to train the ANN, while the validation set allow to stop the training process at the right moment in order to avoid the overfitting of the ANN-model. Using the trained ANN-based model instead of numerical simulations can speed up the calculation process.

3. Results and discussion

3.1. Inverse problem i – Identification of the ABDR stiffness parameters

The first inverse problem (IP1) aimed to identify the effective stiffness components of the ABDR matrix for a homogenized corrugated cardboard plate, based on synthetic reference data. These reference values originated from a perturbed 3D finite element model incorporating realistic imperfections such as 5 % variability in material stiffnesses and geometrical dimensions. The optimization was initialized using stiffness values computed for the idealized geometry (i.e., without imperfections).

The vector of design variables included ten independent components of the ABDR matrix:

$$\{A_{11}, A_{22}, A_{12}, A_{33}, D_{11}, D_{22}, D_{12}, D_{33}, R_4, R_5\} \tag{22}$$

3.1.1. Convergence behavior

The optimization process exhibited a smooth and monotonic reduction in the objective function value, spanning nearly six orders of magnitude (from 1 to below 10^{-6}) as shown in Fig. 7. This indicates both the accuracy of the inverse model and the numerical stability of the algorithm used.

3.1.2. Evolution of the identified parameters

Figs. 8 and 9 illustrate the evolution of raw and normalized stiffness parameters, respectively. All components gradually stabilized after approximately 40–50 iterations. Several stiffness components experienced significant changes compared to their initial (idealized) values.

- Membrane stiffness components A_{11}, A_{22}, A_{33} increased by more than 100 %, indicating low sensitivity or strong compensation for geometric and material imperfections.

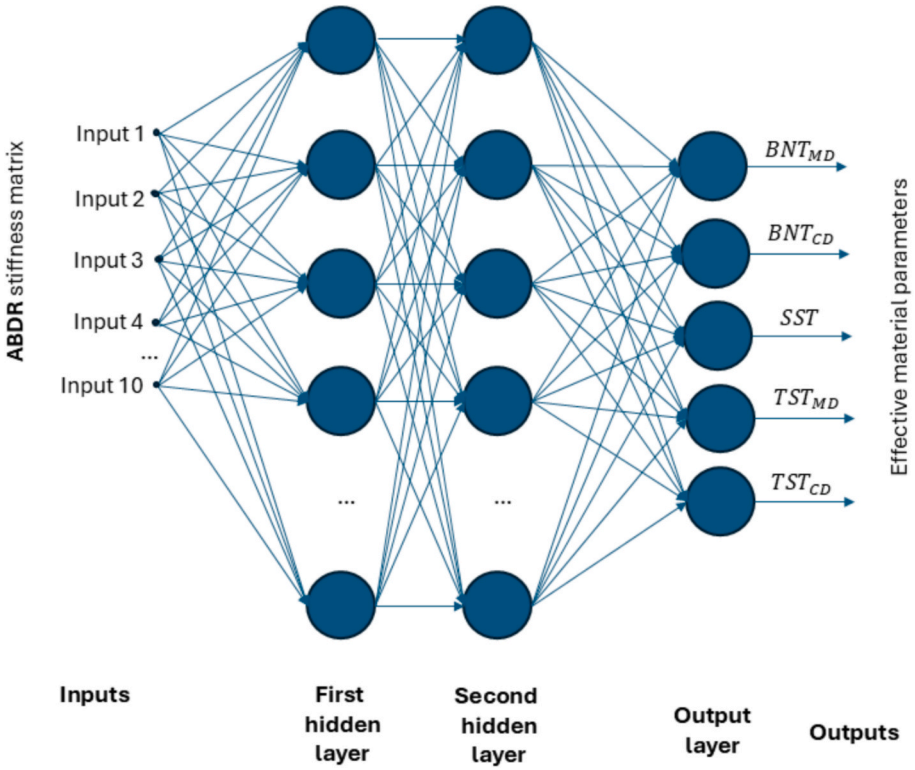

Fig. 6. ANN-based model for prediction of effective material properties.

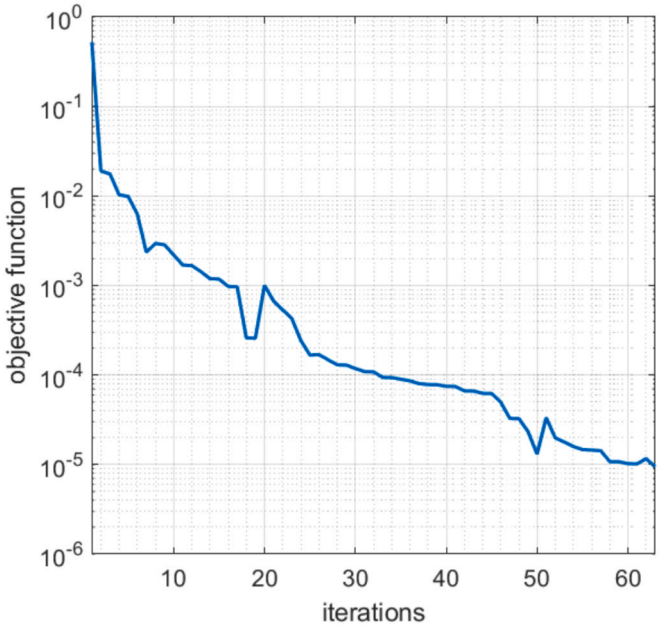

Fig. 7. Convergence history of the objective function during inverse identification of **ABDR** stiffness parameters – Inverse Problem I.

- Bending stiffness components $D_{11}, D_{22}, D_{12}, D_{33}$ exhibited relatively modest changes (within 30 %).
- Shear stiffness components R_4 decreased, reflecting the softening of transverse shear behavior due to out-of-plane imperfections.

3.1.3. Sensitivity analysis

The parameter sensitivity was evaluated at each iteration and is summarized using box plots in Fig. 10. *The distribution shows that the bending stiffness terms—especially D_{33}, D_{22}—consistently had the highest influence on the objective function. Membrane stiffnesses A_{ij} showed negligible sensitivity throughout, which may be explained by the dominance of bending deformations in the loading configurations used. Interestingly, the shear terms R_4 and R_5 exhibited wide spread (outliers present), indicating moderate but variable influence depending on the iteration step. These findings are consistent with the results of Garbowski et al.* [60]*, who demonstrated via designed experiments that the effective mechanical response of corrugated boards is governed predominantly by bending and transverse shear behavior, with relatively minor contribution from membrane terms.*

3.1.4. Discussion

The optimization procedure successfully recovered the effective **ABDR** stiffness matrix that replicates the behavior of a realistic, perturbed 3D model using only simplified plate-level parameters. The strong deviation between the final and initial parameter values confirms the critical importance of calibration, especially when imperfections or nonlinearities are present at the microscale.

The steep and stable convergence of the objective function (Fig. 7), along with coherent parameter trends (Figs. 8–9), confirms that the solution is robust and well-posed. The observed low sensitivity of in-plane stiffness terms and high sensitivity of bending terms further supports the use of inverse identification focused on bending-dominated tests.

Finally, the effectiveness of the approach was confirmed through multiple initializations (see Table 3), which all converged to consistent solutions with only minor variance (within 5 %), reinforcing the uniqueness and reliability of the identified stiffness vector.

Additionally, the sensitivity analysis conducted during optimization, averaged over all iterations, reveals that the most influential parameters were D_{33}, D_{22}, and D_{12}. This observation aligns closely with the findings reported by Garbowski et al. [60], where a systematic sensitivity analysis demonstrated that bending stiffnesses and bending-twisting coupling terms are the dominant factors influencing the global mechanical response of corrugated structures. The consistency between our

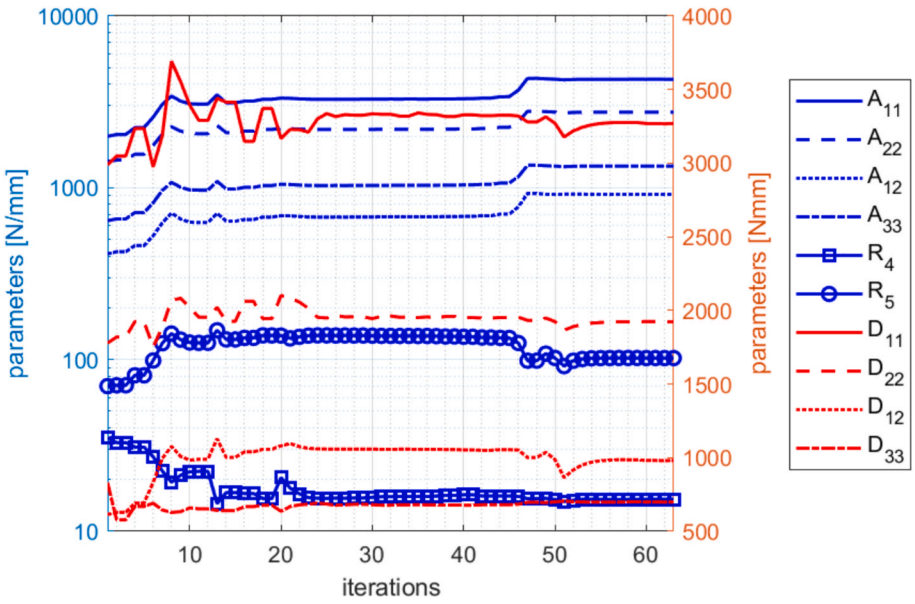

Fig. 8. Evolution of raw **ABDR** stiffness parameters across optimization iterations.

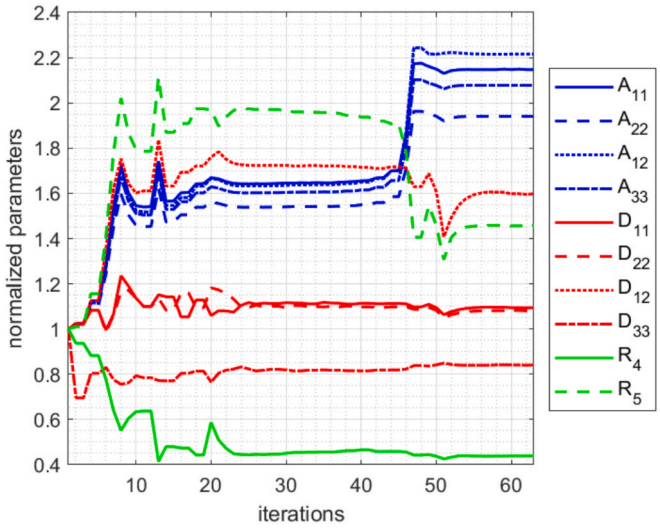

Fig. 9. Evolution of normalized **ABDR** stiffness parameters relative to their initial values.

optimization-based sensitivity trends and those independently obtained via designed sensitivity experiments further validates the robustness and physical realism of the inverse identification process presented herein.

3.2. *Inverse problem II – Identification of the microstructural parameters*

In the second inverse problem (IP2a), the objective was to reconstruct the geometry and material properties of the corrugated board's constituent layers based on the target stiffness values obtained in the first inverse problem (IP1). The identified target ABDR matrix served as a reference for calibrating a parameterized analytical model that takes as input the fluting geometry (period and height) and the mechanical parameters of the top liner, fluting, and bottom liner.

The full set of design variables included: \.

- geometry:
  - fluting period P [mm]
  - fluting height H [mm];
- layer 1 (top liner):
  - thickness TH_1 [mm]
  - Young's moduli E_1^{MD}, E_1^{CD} [MPa];
- layer 2 (fluting):
  - thickness TH_2 [mm]
  - Young's moduli E_2^{MD}, E_2^{CD} [MPa];
- layer 3 (bottom liner):
  - thickness TH_3 [mm]
  - Young's moduli E_3^{MD}, E_3^{CD} [MPa]

3.2.1. *Convergence behavior*

Fig. 11 presents the convergence of the objective function over the optimization process. A clear and rapid decrease is observed—from values exceeding 1.0 to less than 10^{-2} within 25 iterations. The nearly monotonic trend, without erratic oscillations, indicates a well-posed problem and a stable descent direction within the interior-point optimization algorithm.

3.2.2. *Parameter evolution*

Fig. 12 shows the absolute values of all design variables throughout the optimization. Parameters are plotted with two y-axes: blue for geometry and thicknesses [mm], and red for elastic moduli [MPa]. The optimization exhibits distinct stages:

- a reduction in H (fluting height) followed by an increase in paper moduli (particularly E_3^{MD}, E_2^{MD}),
- strong adjustments in the fluting and bottom liner properties,
- rapid convergence of paper thicknesses after 10–15 iterations.

Fig. 13 presents the same evolution in normalized form, offering clearer insight into the relative magnitude of parameter changes. Notably: (i) E_2^{MD} decreases by nearly 70 %, (ii) H fluctuates mildly, (iii) most other parameters converge within $\pm$ 5 % of their initial values.

3.2.3. *Sensitivity analysis*

The sensitivity analysis (Fig. 14) reveals that the most influential parameter throughout the optimization was the fluting height H. It consistently showed the highest median sensitivity and wide variability, indicating its dominant role in adjusting the out-of-plane stiffness. Other influential parameters include: (a) E_1^{MD}, E_2^{CD}, and E_3^{MD}, (b) modest

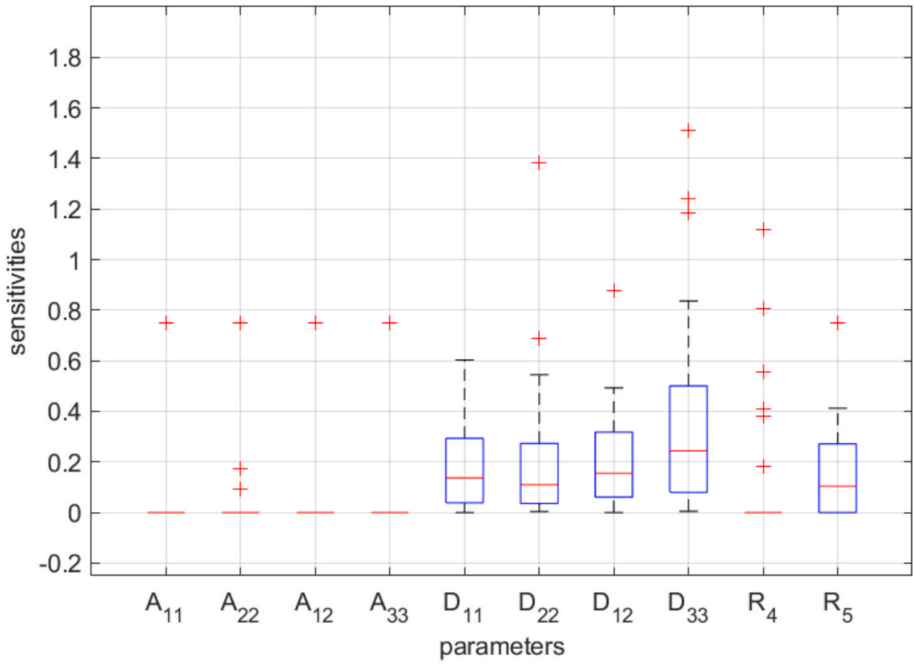

Fig. 10. Box plot of parameter sensitivities computed throughout the optimization iterations.

Table 3
Identified ABDR stiffness parameters from IP1 optimization with multi-start initialization: mean values and standard deviations.

A_{11}	A_{22}	A_{12}	A_{33}	R_4	R_5	D_{11}	D_{22}	D_{12}	D_{33}
[N/mm]						[Nmm]			
4277.4	2754.1	915.1	1335.8	3269.5	1923.3	981.2	698.9	15.4	101.9
± 127.0	± 79.8	± 25.2	± 38.9	± 84.2	± 51.6	± 29.7	± 20.9	± 0.41	± 2.81

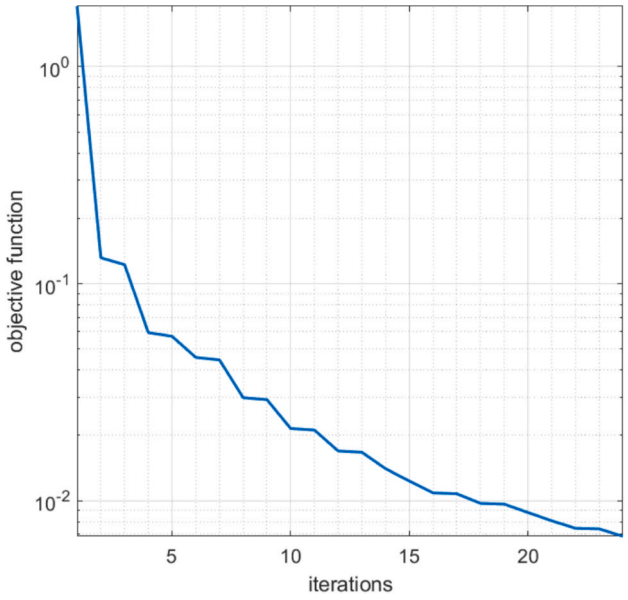

Fig. 11. Objective function convergence during the identification of geometric and material parameters (logarithmic scale) – Inverse Problem II.

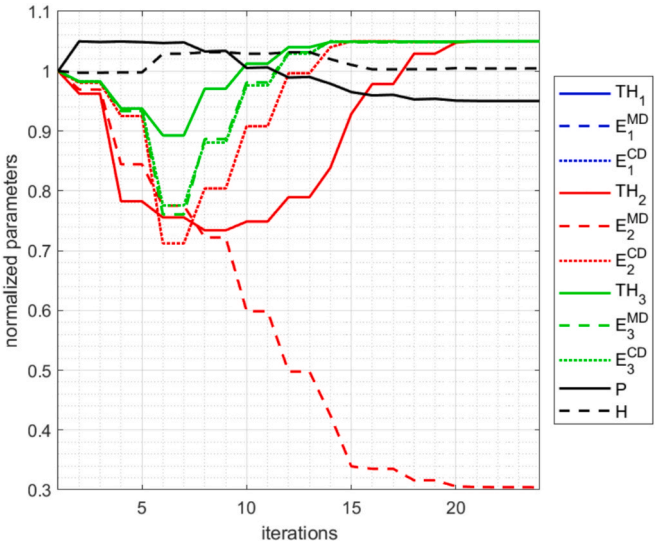

Fig. 12. Evolution of parameter values during optimization.

influence from thicknesses TH_2, TH_3, (c) low influence from E_1^{CD}, E_3^{CD}, and P.

This profile confirms that while geometry—particularly wave height—drives the global bending stiffness, the material properties in MD direction of fluting and liners act as fine-tuning elements.

3.2.4. Discussion

The results of the second inverse problem (IP2) confirm that it is possible to reliably reconstruct the microstructural parameters of corrugated board by calibrating a simplified analytical model to match global stiffness characteristics. The optimization process demonstrated good numerical conditioning, as evidenced by the smooth and monotonic convergence of the objective function. The recovered parameter set yields an effective stiffness matrix that closely approximates the

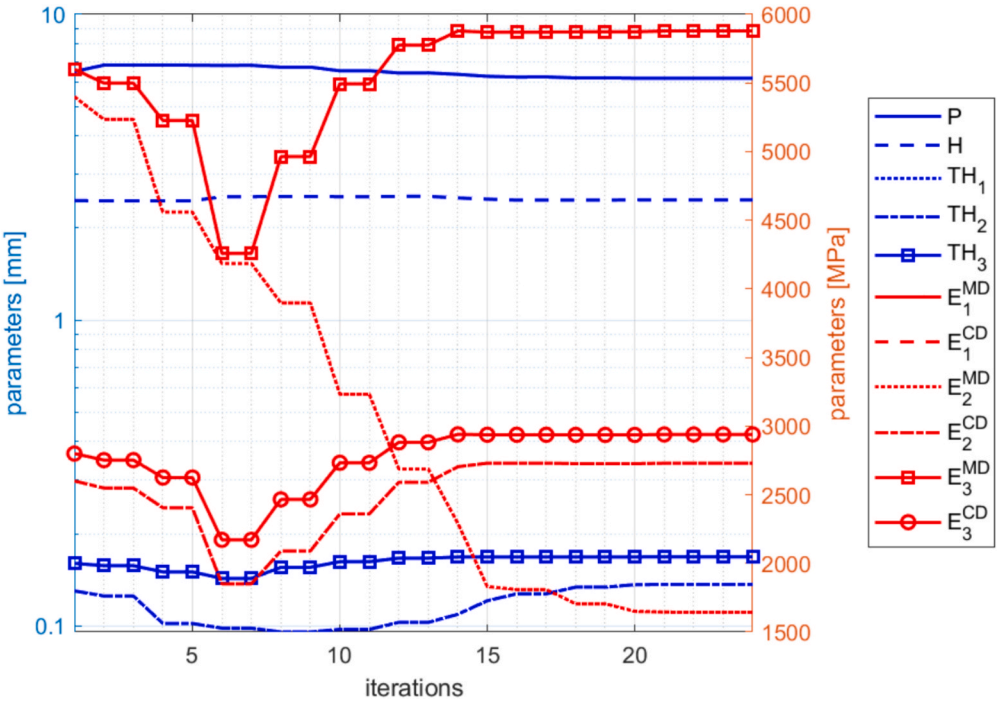

Fig. 13. Normalized evolution of parameters during optimization (relative to initial values).

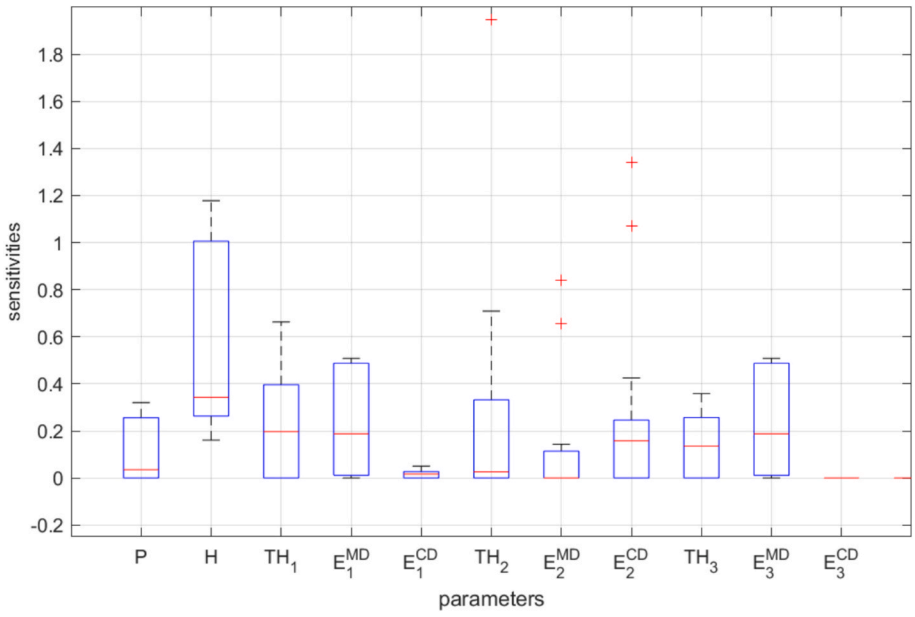

Fig. 14. Box plots of parameter sensitivities over the optimization history in IP2.

target values previously identified through inverse homogenization in IP1.

The parameter evolution observed during optimization provides valuable insight into how different physical quantities influence the macroscopic behavior of the structure. The fluting height H emerged as a critical variable, undergoing noticeable adjustments and exhibiting the highest sensitivity across the iterations. This confirms its fundamental role in controlling bending stiffness and structural inertia, a fact long recognized in the mechanics of sandwich and corrugated panels. Although the fluting period P was free to vary, its influence was relatively minor in comparison, suggesting that under given geometric constraints, period variations play a secondary role in stiffness tuning.

Equally significant was the role of the elastic moduli in the machine direction (MD), particularly for the fluting and bottom liner layers. The optimizer adjusted these parameters in a coordinated way, effectively compensating for the limitations imposed by fixed or weakly sensitive geometric variables. In contrast, moduli in the cross direction (CD) showed lower sensitivities, except for the fluting layer where transverse stiffness appeared to affect the shear response of the plate. This agrees with physical intuition, as the fluting, being highly anisotropic and spatially curved, contributes disproportionately to both bending and shear stiffness components, especially those related to coupling effects.

An interesting observation is the relative stability of the thickness parameters. Although they were included in the design space, their

influence was less pronounced than initially expected. This suggests that, within realistic bounds, the optimizer preferred to adjust stiffness by modulating the modulus rather than the cross-sectional dimensions. This behavior may reflect the nonlinear and geometry-sensitive scaling of flexural rigidity with respect to thickness, and possibly the smoother influence of modulus changes on the target stiffness metrics used in the objective function.

Furthermore, the consistency of parameter trajectories and the clear dominance of a few key variables in the sensitivity analysis underscore the well-posed nature of the inverse problem and the robustness of the adopted formulation. The optimization did not exhibit pathological behavior such as parameter drift or degeneracy, which often complicates inverse identification in over-parameterized systems. Instead, it converged to a physically meaningful and interpretable solution, in which fluting geometry and directional stiffnesses were adjusted in a balanced and effective manner. Importantly, the use of a multi-start strategy confirmed that the optimization consistently converged to the same solution (see Table 4), with only minor discrepancies attributable to the chosen convergence tolerances and stopping criteria.

Overall, the findings from IP2 strongly support the feasibility of using reduced-order plate models for back-calculating internal structural parameters of corrugated cardboard. The results also illustrate the interdependence between geometry and material properties, and how these two domains interact within the optimization framework to minimize deviation from experimentally informed target stiffness values. This approach opens the door to more efficient characterization workflows in industrial or design settings, where full-scale 3D simulations or extensive experimental campaigns may be impractical.

3.3. ANN model performance results and discussion

In this study, it is proposed to replace the numerical simulations by a trained ANN in order to speed up the calculation during optimization process. Table 5 shows three variants of the tested ANNs for prediction of the effective material parameters. Variant 1 do not include any neuron in the hidden layer. It means that such ANN model has only the input layer with 10 inputs and the output layer with 5 neurons (each one related to one output – one material parameter). Variant 2 includes one hidden layer with 10 neurons while Variant 3 includes two hidden layer with 10 neurons at each hidden layer.

The training process of the ANN models were performed 100 times for each variant of the ANN structure. The Levenberg-Marquardt method was adopted as the training procedure. The dataset used for training contained 2000 cases coming from numerical simulations and was divided into training set (1400 cases), validation set (300 cases), and test set (300 cases). In order to evaluate the performance of the ANN the root means squared error (RMSE) is defined as follows:

$$RMSE = \sqrt{\frac{\sum_{i=1}^{N} (\hat{y} - y)^2}{N}} \tag{23}$$

where $\hat{y}$ denotes the expected value of the ANN output, y is the obtained value of the ANN output and N is the number the data for testing. After 100 times training processes, the average values of the ANN performance for each output for three variants of the ANN structures are presented in Table 6. One can conclude that each tested ANN model gives very accurate results, while the best one are obtained for the Variant 3 with 2 hidden layers.

Table 5
Structure of artificial neural network models with tangent sigmoidal transfer functions in hidden layers and linear transfer function in the output layer.

	Number of neurons in the first hidden layer	Number of neurons in the second hidden layer
Variant 1	0	0
Variant 2	10	0
Variant 3	10	10

In all previous tests, the tangent sigmoid was applied as the transfer function in the hidden layers. Now, the transfer function employed can be tested. The number of neurons was the same as in Variant 3 (10 neurons both at the first and second hidden layers). We applied the following transfer functions in the hidden layers:

- Variant 4 – linear function,
- Variant 5 – logistic function,
- Variant 6 – ReLU (*Rectified Linear Unit*).

In the output layer, the linear function was kept as the transfer function. The results are shown in Table 7. One can notice that the best results were obtained for Variant 4 (with linear transfer functions in hidden layers). However, the results are very close to the results obtained for Variant 3 (with tangent sigmoidal transfer functions in hidden layers).

The speed-up benefit of using ANN was evaluated based on 100 representative cases. The average computation time for the ANN model was 0.0037 s, compared to 24.5 s for the corresponding FE model computations. This result demonstrates a substantial computational advantage of the ANN model over the traditional FE approach, with an average speed-up factor of approximately 6600 times. Such a dramatic reduction in computation time is beneficial for applications requiring real-time or large-scale simulations, such as optimization tasks, uncertainty quantification, or integration into digital twin frameworks, what perfectly fits the methodology presented in this paper.

4. Conclusions

This study introduced a novel inverse-based, multi-step numerical homogenization framework for the mechanical characterization of converted corrugated board, accounting for both the anisotropy and imperfections induced during production. By combining detailed 3D finite element simulations, simplified homogenized shell models, and optimization-based inverse analyses, the proposed methodology enables the derivation of effective stiffness parameters that realistically reflect conversion-related issues such as micro-damage, adhesive effects, and geometric irregularities.

The two-stage inverse procedure successfully retrieved the composite stiffness matrix of the converted board, showing important deviations from the idealized configuration. This highlights the necessity of considering production-related imperfections in computational modeling. The iterative updating of fluting geometry and paper properties using numerical homogenization allowed for accurate calculation of real-world board characteristics, proving that indirect inverse

Table 4
Identified geometric and material parameters from IP2 optimization with multi-start initialization: mean values and standard deviations.

P	H	TH_1	TH_2	TH_3	E_1^{MD}	E_1^{CD}	E_2^{MD}	E_2^{CD}	E_3^{MD}	E_3^{CD}
[mm]					[MPa]					
6.18	2.47	0.168	0.136	0.168	5878.7	2939.2	1643.1	2729.3	5878.7	2939.2
± 0.17	± 0.07	± 0.005	± 0.004	± 0.005	± 166.4	± 81.1	± 47.9	± 77.9	± 167.3	± 83.5

Table 6
Results of the ANNs performance (average RMSE) for three tested variants of the ANN structure model.

Output	BNT in MD	BNT in CD	SST	TST in MD	TST in CD
Variant 1	$1.12 \bullet 10^{-4}$	$1.08 \bullet 10^{-4}$	$1.16 \bullet 10^{-4}$	$1.06 \bullet 10^{-4}$	$1.19 \bullet 10^{-4}$
Variant 2	$1.40 \bullet 10^{-5}$	$1.39 \bullet 10^{-5}$	$1.36 \bullet 10^{-5}$	$1.36 \bullet 10^{-5}$	$1.42 \bullet 10^{-5}$
Variant 3	$1.14 \bullet 10^{-5}$	$1.10 \bullet 10^{-5}$	$1.18 \bullet 10^{-5}$	$1.20 \bullet 10^{-5}$	$1.13 \bullet 10^{-5}$

Table 7
Results of the ANNs performance (average RMSE) for three tested variants of the applied transfer functions in hidden layers.

Output	BNT in MD	BNT in CD	SST	TST in MD	TST in CD
Variant 4	$1.06 \bullet 10^{-5}$	$1.09 \bullet 10^{-5}$	$1.04 \bullet 10^{-5}$	$1.10 \bullet 10^{-5}$	$1.03 \bullet 10^{-5}$
Variant 5	$1.82 \bullet 10^{-5}$	$1.90 \bullet 10^{-5}$	$1.66 \bullet 10^{-5}$	$1.82 \bullet 10^{-5}$	$1.88 \bullet 10^{-5}$
Variant 6	$3.93 \bullet 10^{-4}$	$4.38 \bullet 10^{-4}$	$3.45 \bullet 10^{-4}$	$3.64 \bullet 10^{-4}$	$4.07 \bullet 10^{-4}$

approaches can effectively replace or supplement physical experiments.

Sensitivity analyses revealed that fluting height and period have a dominant influence on the board's mechanical performance, also bending behavior shown its critical role in design and optimization.

Furthermore, the study in the paper, shows that the incorporation of an artificial neural network significantly reduces computational time without compromising prediction accuracy. This makes the methodology applicable in time-critical applications such as digital twin environments, optimization loops or online laboratory/production performance predictions of cardboards.

The proposed framework is not limited to a specific board configuration or test type and could be extended to other layered or structurally complex materials. In summary, the study offers a reliable and computationally efficient method for characterizing the mechanical properties of converted corrugated board, which can be one of the tools for more innovative design, analysis, and simulation practices in the packaging industry.

CRediT authorship contribution statement

Tomasz Garbowski: Writing – review & editing, Writing – original draft, Visualization, Validation, Supervision, Software, Project administration, Methodology, Investigation, Formal analysis, Conceptualization. **Aram Cornaggia:** Writing – review & editing, Writing – original draft, Validation, Investigation, Data curation. **Tomasz Gajewski:** Writing – review & editing, Writing – original draft, Visualization, Validation, Supervision, Software, Project administration, Methodology, Investigation, Formal analysis, Conceptualization. **Jakub K. Grabski:** Writing – original draft, Writing – review & editing, Validation, Visualization, Software, Investigation, Formal analysis. **Damian Mrówczyński:** Writing – review & editing, Writing – original draft, Validation, Software, Investigation, Data curation.

Declaration of competing interest

The authors declare that they have no known competing financial interests or personal relationships that could have appeared to influence the work reported in this paper.

Data availability

Data will be made available on request.

References

[1] Simon JW. A review of recent trends and challenges in computational modeling of paper and paperboard at different scales. Arch Comput Meth Eng 2020;28(6):2409–28. https://doi.org/10.1007/s11831-020-09460-y.

[2] Coffin DW. Historical perspectives of corrugated box testing. Tappi J 2020;19(3):161–73. https://doi.org/10.32964/TJ19.3.173.

[3] Pevec P, Kapun T, Gregor-Svetec D. Recyclability of intelligent cardboard packaging. Sustainability 2025;17(7):2924. https://doi.org/10.3390/su17072924.

[4] Di Russo FM, Desole MM, Gisario A, Barletta M. Evaluation of wave configurations in corrugated boards by experimental analysis (EA) and finite element modeling (FEM): the role of the micro-wave in packaging design. Int J Adv Manuf Technol 2023;126(6):4963–82. https://doi.org/10.1007/s00170-023-11397-y.

[5] Garbowski T, Gajewski T, Grabski JK, Mrówczyński D, Cornaggia A. Identification of material and structural parameters of corrugated board in production and converting processes. In: Trovalusci P, Sadowski T, Ibrahimbegovic A (Eds), Multiscale and Multiphysics Modelling for Advanced and Sustainable Materials 2025. Accepted.

[6] Mrówczyński D, Gajewski T, Cornaggia A, Garbowski T. Impact of temperature and humidity on key mechanical properties of corrugated board. Appl Sci 2024;14(24):12012. https://doi.org/10.3390/app142412012.

[7] Biancolini ME, Brutti C. Numerical and experimental investigation of the strength of corrugated board packages. Packag Technol Sci 2003;16(2):47–60. https://doi.org/10.1002/pts.609.

[8] Biancolini ME. Evaluation of equivalent stiffness properties of corrugated board. Compos Struct 2005;69(3):322–8. https://doi.org/10.1016/j.compstruct.2004.07.014.

[9] Garbowski T, Gajewski T. Determination of transverse shear stiffness of sandwich panels with a corrugated core by numerical homogenization. Materials 2021;14(8):1976. https://doi.org/10.3390/ma14081976.

[10] Ngira Aduke R, Venter MP, Coetzee CJ. An analysis of numerical homogenisation methods applied on corrugated paperboard. Math Comput Appl 2023;28(2):46. https://doi.org/10.3390/mca28020046.

[11] Buannic N, Cartraud P, Quesnel T. Homogenization of corrugated core sandwich panels. Compos Struct 2003;59(3):299–312. https://doi.org/10.1016/S0263-8223(02)00246-5.

[12] Talbi N, Batti A, Ayad R, Guo Y. An analytical homogenization model for finite element modelling of corrugated cardboard. Compos Struct 2009;88(2):280–9. https://doi.org/10.1016/j.compstruct.2008.04.008.

[13] Tran LV, Ferreira AJM, Nguyen-Xuan H. Isogeometric analysis of functionally graded plates using higher-order shear deformation theory. Compos B Eng 2013;51(8):368–83. https://doi.org/10.1016/j.compositesb.2013.02.045.

[14] Al Jahwari F, Naguib HE. Analysis and homogenization of functionally graded viscoelastic porous structures with a higher order plate theory and statistical based model of cellular distribution. App Math Model 2016;40(3):2190–205. https://doi.org/10.1016/j.apm.2015.09.038.

[15] Khakalo S, Niiranen J. Anisotropic strain gradient thermoelasticity for cellular structures: plate models, homogenization and isogeometric analysis. J Mech Phys Solids 2020;134(1):103728. https://doi.org/10.1016/j.jmps.2019.103728.

[16] Georgiades AV, Kalamkarov AL, Challagulla KS. Asymptotic homogenization model for generally orthotropic reinforcing networks in smart composite plates. Smart Materials and Structures 2006; 15(8): 1197. https://doi.org/ 10.1088/0964-1726/15/5/006.

[17] Huang Z, Xing Y, Gao Y. Two-scale asymptotic homogenization method for composite kirchhoff plates with in-plane periodicity. Aerospace 2022;9(12):751. https://doi.org/10.3390/aerospace9120751.

[18] Helfen CE, Diebels S. A numerical homogenisation method for sandwich plates based on a plate theory with thickness change. ZAMM –. J Appl Math Mech 2012;93(2–3):113–25. https://doi.org/10.1002/zamm.201100173.

[19] Helfen CE, Diebels S. Computational homogenisation of composite plates: consideration of the thickness change with a modified projection strategy. Comput Math Appl 2014;67(5):1116–29. https://doi.org/10.1016/j.camwa.2013.12.017.

[20] Garbowski T, Szymczak-Graczyk A, Cornaggia A. Sectional homogenization with a general nonlinear constitutive law for corrugated board analysis. In: Papadrakakis M, Papapdopoulos V, Stefanou G (eds), Proceedings of the 6th ECCOMAS Thematic Conference on Uncertainty Quantification in Computational Sciences and Engineering, UNCECOMP 2025. In print.

[21] Inverse TA, Theory P. Philadelphia. USA: Siam; 2005.

[22] Mróz Z, Stavroulakis GE. Parameter identification of materials and structures. 2005, Udine, Italy: Springer.

[23] Waszczyszyn Z, Ziemiański L. Neural networks in mechanics of structures and materials – new results and prospects of applications. Comput Struct 2001;79 (22–25):2261–76. https://doi.org/10.1016/S0045-7949(01)00083-9.
[24] Buljak V, Cocchetti G, Cornaggia A, Garbowski T, Maier G, Novati G. Materials Mechanical Characterizations and Structural Diagnoses by Inverse Analyses. In: Voyadjis GZ (ed) Handbook of Damage Mechanics. 2015, New York, USA: Springer. 619-642. Doi: 10.1007/978-1-4614-5589-9_33.
[25] Garbowski T, Maier G, Novati G. On calibration of orthotropic elastic-plastic constitutive models for paper foils by biaxial tests and inverse analyses. Struct Multidiscip Optim 2012;46(1):111–28. https://doi.org/10.1007/s00158-011-0747-3.
[26] Östlund S, Niskanen K (Eds). Mechanics of Paper Products. 2021, Amsterdam, The Netherlands: De Gruyter.
[27] Nienke T, Kwade A, Eggerath D. Influence of moisture, temperature and bleaching on the mechanical properties of coated fiber-based substrates. Coatings 2022;12 (9):1287. https://doi.org/10.3390/coatings12091287.
[28] Wang D. Elastic modulus prediction of corrugating medium under different temperature and relative humidity. IOP Conf Ser: Mater Sci Eng 2018;439(4): 042043. https://doi.org/10.1088/1757-899X/439/4/042043.
[29] Marin G, Srinivasa P, Nygårds M, Östlund S. Experimental and finite element simulated box compression tests on paperboard packages at different moisture levels. Packag Technol Sci 2021;34(4):229–43. https://doi.org/10.1002/pts.2554.
[30] Cornaggia A, Gajewski T, Knitter-Piątkowska A, Garbowski T. Influence of humidity and temperature on mechanical properties of corrugated board-numerical investigation. BioResources 2023;18(4):7490–509. https://doi.org/10.15376/biores.18.4.7490-7509.
[31] Aboura Z, Talbi N, Allaoui S, Benzeggagh ML. Elastic behavior of corrugated cardboard: experiments and modeling. Compos Struct 2004;63(1):53–62. https://doi.org/10.1016/S0263-8223(03)00131-4.
[32] Di Russo FM, Desole MP, Gisario A, Genovesi A, Barletta M. Study and design of corrugated cardboard trays with microwaves by experimental analysis (EA) and finite element methods (FEM). Packag Technol Sci 2024;37(9):857–74. https://doi.org/10.1002/pts.2827.
[33] Cornaggia A, Mrówczyński D, Gajewski T, Knitter-Piątkowska A, Garbowski T. Advanced numerical analysis of transport packaging. Appl Sci 2024;14(24):11932. https://doi.org/10.3390/app142411932.
[34] Garbowski T, Gajewski T, Grabski JK. Estimation of the compressive strength of corrugated cardboard boxes with various openings. Energies 2021;14(1):155. https://doi.org/10.3390/en14010155.
[35] Garbowski T, Gajewski T, Grabski JK. Estimation of the compressive strength of corrugated cardboard boxes with various perforations. Energies 2021;14(4):1095. https://doi.org/10.3390/en14041095.
[36] Suarez B, Muneta MLM, Sanz-Bobi JD, Romero G. Application of homogenization approaches to the numerical analysis of seating made of multi-wall corrugated cardboard. Compos Struct 2021;262(4):113642. https://doi.org/10.1016/j.compstruct.2021.113642.
[37] Beck M, Fischerauer G. Modeling warp in corrugated cardboard based on homogenization techniques for in-process measurement applications. Appl Sci 2022;12(3):1684. https://doi.org/10.3390/app12031684.
[38] Tanninen P, Leminen V, Kainusalmi M, Varis J. Effect of process parameter variation on the dimensions of press-formed paperboard trays. BioResources 2016; 11(1):140–58. https://doi.org/10.15376/biores.11.1.140-158.
[39] Garbowski T, Gajewski T, Mrówczyński D, Jędrzejczak R. Crushing of single-walled corrugated board during converting: experimental and numerical study. Energies 2021;14(11):3203. https://doi.org/10.3390/en14113203.
[40] Johst P, Kaeppeler U, Seibert D, Kucher M, Böhm R. Investigation of different cardboard materials under impact loads. BioResources 2023;18(1):1933–47. https://doi.org/10.15376/biores.18.1.1933-1947.
[41] Awais M, Tanninen P, Leppänen T, Matthews S, Sorvari J, Varis J, et al. A computational and experimental analysis of crease behavior in press forming process. Procedia Manuf 2018;17(1):835–42. https://doi.org/10.1016/j.promfg.2018.10.135.
[42] Leminen V, Tanninen P, Pesonen A, Varis J. Effect of mechanical perforation on the press-forming process of paperboard. Procedia Manuf 2019;38(1):1402–8. https://doi.org/10.1016/j.promfg.2020.01.148.
[43] Jamsari MA, Kueh C, Gray-Stuart EM, Dahm K, Bronlund JE. Modelling the impact of crushing on the strength performance of corrugated fibreboard. Packag Technol Sci 2020;33(4–5):159–70. https://doi.org/10.1002/pts.2494.
[44] Ayrilmis N, Candan Z, Hiziroglu S. Physical and mechanical properties of cardboard panels made from used beverage carton with veneer overlay. Mater Des 2008;29(10):1897–903. https://doi.org/10.1016/j.matdes.2008.04.030.
[45] Mrówczyński D, Knitter-Piątkowska A, Garbowski T. Numerical homogenization of single-walled corrugated board with imperfections. Appl Sci 2022;12(19):9632. https://doi.org/10.3390/app12199632.
[46] Marek A, Garbowski T. Homogenization of sandwich panels. Comput Assist Methods Eng Sci 2015;22(1):39–50.
[47] Garbowski T, Knitter-Piątkowska A, Winiarski P. Simplified modelling of the edge crush resistance of multi-layered corrugated board: experimental and computational study. Materials 2023;16(1):458. https://doi.org/10.3390/ma16010458.
[48] ISO 187:2022 Paper, Board and Pulps—Standard Atmosphere for Conditioning and Testing and Procedure for Monitoring the Atmosphere and Conditioning of Samples. 2022, Geneva, Switzerland: International Standard ISO.
[49] TAPPI T402 sp-21 Standard Conditioning and Testing Atmospheres for Paper, Board, Pulp Handsheets, and Related Products, Test Method TAPPI/ANSI T 402 sp-21. 2021, Atlanta, USA: TAPPI.
[50] FEFCO Testing Method No. 8 Edgewise Crush Resistance of Corrugated Fiberboard. 1997, Brussels, Belgium: European Federation of Corrugated Board Manufacturers.
[51] Dassault Systèmes. Abaqus Unified FEA® Software. Available online: https://www.3ds.com/products-services/simulia/products/abaqus (accessed on 28 April 2025).
[52] Fiacco AV, McCormick GP. Nonlinear Programming: Sequential Unconstrained Minimization Techniques. 1968, Chichester, UK: Wiley.
[53] Byrd RH, Hribar ME, Nocedal J. An interior point algorithm for large-scale nonlinear programming. SIAM J Optim 1999;9(4):877–900. https://doi.org/10.1137/S1052623497325107.
[54] Wächter A, Biegler LT. On the implementation of an interior-point filter line-search algorithm for large-scale nonlinear programming. Math Program 2006;106(1): 25–57. https://doi.org/10.1007/s10107-004-0559-y.
[55] Zarringol M, Patel VI, Liang QQ. Artificial neural network model for strength predictions of CFST columns strengthened with CFRP. Eng Struct 2023;281(4): 115784. https://doi.org/10.1016/j.engstruct.2023.115784.
[56] Owusu-Danquah JS, Bseiso A, Allena S, Duffy SF. Artificial neural network algorithms to predict the bond strength of reinforced concrete: coupled effect of corrosion, concrete cover, and compressive strength. Constr Build Mater 2022;350 (10):128896. https://doi.org/10.1016/j.conbuildmat.2022.128896.
[57] Nguyen QH, Ly H-B, Nguyen T-A, Phan V-H, Nguyen LK, Tran VQ. Investigation of ANN architecture for predicting shear strength of fiber reinforcement bars concrete beams. PLoS One 2021;16(4):e0247391. https://doi.org/10.1371/journal.pone.0247391.
[58] Asteris PG, Argyropoulos I, Cavaleri L, Rodrigues H, Varum H, Thomas J, et al. Masonry compressive strength prediction using artificial neural networks. Commun Comput Information Sci 2019;962(1):200–24. https://doi.org/10.1007/978-3-030-12960-6_14.
[59] Spanu P, Abaza BF. Tensile strength prediction of fiberglass polymer composites using artificial neural network model. Materiale Plastice 2022;59(2):111–8. https://doi.org/10.37358/MP.22.2.5590.
[60] Garbowski T, Pozorska J, Pozorski Z. Mechanical characterization of corrugated board: sensitivity analysis in design of experiments. Thin-Walled Struct 2025;216 (A):113671. https://doi.org/10.1016/j.tws.2025.113671.